A&A 468, 663–677 (2007)
DOI: 10.1051/0004-6361:20077220

Astronomy & Astrophysics

Behavior of Li abundances in solar-analog stars

Evidence for line-width dependence⋆,⋆⋆

Y. Takeda, S. Kawanomoto, S. Honda, H. Ando, and T. Sakurai

National Astronomical Observatory of Japan, 2-21-1 Osawa, Mitaka, Tokyo 181-8588, Japan
e-mail: takedayi@cc.nao.ac.jp

Received 2 February 2007 / Accepted 5 March 2007

ABSTRACT

Context. It is known that the surface lithium abundances of field solar-analog G dwarfs show a large dispersion of ≳2 dex (among which our Sun is located at the lower end) despite the similarity of stellar parameters, and planet-host stars tend to show comparatively lower Li abundances in the narrow $T_{\rm eff}$ range.
Aims. To investigate the reason for these phenomena, an extensive study of Li abundances and their dependence on stellar parameters was carried out for a homogeneous sample of 118 selected solar analogs based on high-dispersion spectra obtained at Okayama Astrophysical Observatory.
Methods. The atmospheric parameters were spectroscopically determined by using the equivalent widths of Fe I and Fe II lines, the ages/masses were estimated from stellar evolutionary tracks, and the width of the macrobroadening (rotation plus macroturbulence) function as well as Li abundances ($A_{\rm Li}$) were established by spectrum-fitting analyses.
Results. The resulting $A_{\rm Li}$ vs. $T_{\rm eff}$ relation revealed a characteristic inverse-triangle-like distribution enclosed by two clear-cut boundaries (the slanted one running from ∼5900 K to ∼5800 K and the vertical one at ∼5700 K), while the Sun is located around its lowest apex. More significantly, $A_{\rm Li}$ in this region of large dispersion was found to closely correlate with the macrobroadening width ($v_{\rm r+m}$), which is considered to be the most important parameter.
Conclusions. With a reasonable assumption that the difference of rotational velocity is mainly responsible for the variety of $v_{\rm r+m}$, we may conclude that the stellar angular momentum plays the decisive role in determining the surface Li abundances of solar-analog stars in the $T_{\rm eff}$ range of ∼5900–5700 K. The low-Li tendency of planet-host stars may thus be interpreted in terms of rotational characteristics.

Key words. stars: abundances – stars: atmospheres – stars: fundamental parameters – stars: late-type – Sun: fundamental parameters

1. Introduction

It is of astrophysical importance to study the abundance of lithium on the surface of late-type (F–G–K) stars; i.e., it in principle provides us with valuable information regarding the past history and the physical mechanism of stellar envelope mixing, since Li nuclei are burned and destroyed when they are conveyed into the hot stellar interior ($T \sim 2.4 \times 10^6$ K). Yet, it is not generally easy to give a reasonable account on its behavior from a theoretical point of view. As a matter of fact, even the surface Li abundances of ordinary field stars similar to our Sun are not well understood and several problems remain unexplained.

First, according to several recent elaborate and extensive studies, solar-type G-dwarfs show a large dispersion of Li abundances amounting to ∼2 dex or more in the effective temperature ($T_{\rm eff}$) range of ∼5500–6000 K (see, e.g., Pasquini et al. 1994; Favata et al. 1996; Chen et al. 2001; Qiu et al. 2001; Mallik et al. 2003; Galeev et al. 2004; Lambert & Reddy 2004). Admittedly, this region corresponds to the transition region in the course of the declining of surface Li abundance ($A_{\rm Li}$) with a lowering of $T_{\rm eff}$ from F through G to K owing to the increase in the efficiency of envelope mixing[1] (i.e., ever deepening of the convection zone). Even so, what mechanism could be responsible for such a large diversity of $A_{\rm Li}$ among similar stars of near-solar $T_{\rm eff}$?

Second, and more interestingly, an important discovery was made by Israelian et al. (2004), who reported that planet-host stars tend to show significantly less $A_{\rm Li}$ than non-planet-host stars in the same $T_{\rm eff}$ range of large dispersion in the $A_{\rm Li}$ vs. $T_{\rm eff}$ diagram[2]. This trend was further confirmed by the follow-up studies of Takeda & Kawanomoto (2005, hereinafter refereed

⋆ Based on observations carried out at Okayama Astrophysical Observatory (Okayama, Japan).

⋆⋆ Tables 2–6 are only available in electronic form at the CDS via anonymous ftp to cdsarc.u-strasbg.fr (130.79.128.5) or via http://cdsweb.u-strasbg.fr/cgi-bin/qcat?J/A+A/468/663

[1] We use the term "efficiency of mixing" as a measure of how Li atoms are effectively conveyed and mixed to the hot inner layer where they are destroyed. Note that two factors may be involved here: the depth of the convection zone (generally deepened with a lowering of $T_{\rm eff}$) and the rate of mixing (or shaking efficiency) in the envelope.

[2] The possibility of Li deficiency in planet-host stars had been argued by King et al. (1997) and Gonzalez & Laws (2000), which was then criticized by Ryan (2000) as unlikely. However, the arguments in these previous studies are based on insufficient observational data as well as a naive parameterization of $A_{\rm Li}$ (simply in terms of $T_{\rm eff}$, age/activity, and [Fe/H], referring to open cluster observations), which now appear to be outdated. In contrast, the work of Israelian et al. (2004) is based on a much larger number of planet-host stars, which we may consider more reliable.

to as Paper II) and Chen & Zhao (2006), though Luck & Heiter (2006) questioned its reality. If the Li abundance at the stellar surface depends on whether a star has a planet or not, what physical process is involved?

Third, $A_{\rm Li}$ in the Sun appears to be located nearly at the lowest end (i.e., an outlier) in the considerable spread exhibited by similar solar-type stars. This tendency has been seen in studies of "solar twins". That is, while several stars are considered to have stellar parameters very close to those of the Sun, such as 18 Sco (Porto de Mello & da Silva 1997), HIP 78399 (King et al. 2005), and HD 98618 (Meléndez et al. 2006), all these show a marked difference from the Sun with respect to the strength of the Li line (i.e., appreciably stronger than the solar case). Is our Sun an anomalous star with regard to Li? Does this have anything to do with the solar-system planets?

Unfortunately, currently accumulated observational Li abundance data of solar-type stars are not yet satisfactory from a quantitative as well as qualitative point of view to answer these questions:

- The number of solar-analog stars in the relevant $T_{\rm eff}$ region with a diversity of $A_{\rm Li}$ is still insufficient. For example, in the recent Li abundance investigations quoted above, the number of stars with $|\Delta T_{\rm eff}| \lesssim 100$–$200$ K (Δ means the difference from the solar value) is ∼20–30 at most, which should be increased up to ∼100 for a statistically more meaningful discussion.
- The precision of stellar parameter determinations in previous work may not have been sufficiently high as to allow a close investigation of the characteristic distribution (if any exists) in the $A_{\rm Li}$ vs. $T_{\rm eff}$ diagram. For instance, we need to have a precision of at least a few tens of K in $T_{\rm eff}$ in order to argue the behavior of Li abundance within the narrow $T_{\rm eff}$ interval of ∼200–300 K. Knowing or establishing other stellar parameters (e.g., $\log g$, age, line width, etc.) as precisely as possible is likewise necessary to investigate their roles in affecting the surface Li.

Considering this situation, we decided to carry out a new systematic Li abundance study for a large number (∼100) of carefully selected solar-analog stars based on our own observational data obtained at Okayama Astrophysical Observatory, while establishing their parameters as accurately as possible so as to achieve a sufficiently high "resolution" in the parameter/abundance space, to understand the behavior of $A_{\rm Li}$ in this peculiar near-solar $T_{\rm eff}$ range.

In Sect. 2, we explain our basic observational data including the properties of the selected solar-analog stars. Section 3 is devoted to the description of stellar parameter determinations, where the atmospheric parameters are established by the spectroscopic method using Fe I/Fe II lines and the age/mass are estimated from stellar evolutionary tracks. In Sect. 4, we describe the spectrum-fitting analyses for evaluating the macrobroadening width (rotation plus macroturbulence) as well as for determining the Li abundance. The discussion on the behaviors of resulting $A_{\rm Li}$ values and their dependence upon various stellar parameters is presented in Sect. 5, followed by conclusions in Sect. 6. Appendix A describes the "solar twin" candidates from our targets.

2. Observational data

Observations were carried out in the 2005–2006 season (2005 September, 2005 November, 2006 February, and 2006 April) by using the HIgh-Dispersion Echelle Spectrograph (HIDES; Izumiura 1999) at the coudé focus of the 188 cm reflector of Okayama Astrophysical Observatory (OAO). Equipped with a 4K × 2K CCD detector at the camera focus, the HIDES spectrograph enabled us to obtain an echellogram covering a wavelength range of 5600–6800 Å with a resolving power of $R \sim 70\,000$ (case for the normal slit width of 200 μm) in the mode of red cross-disperser. This wavelength region was chosen so as to cover the important Li I 6708 line as well as the green-yellow range including a number of Fe I/Fe II lines.

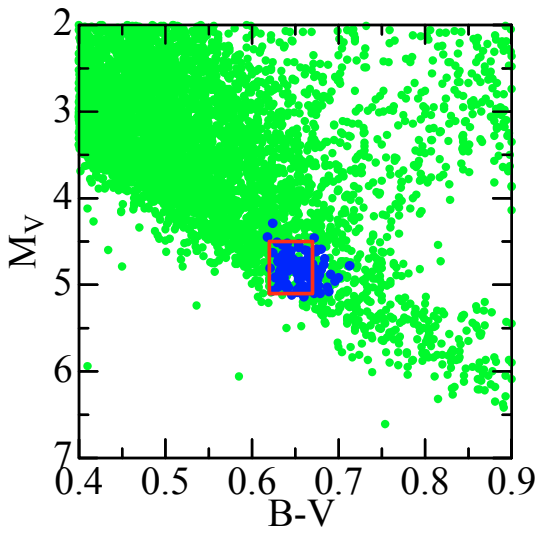

Fig. 1. Plot of the 118 solar-analogs (target stars in this study) on the HR diagram (M_V vs. $B-V$), which were selected from the stars listed in the Hipparcos Catalogue (ESA 1997) also depicted here as thin backgrounds. The rectangle shows the region of $4.5 < M_V < 5.1$ and $0.62 < B-V < 0.67$.

As our solar-analog targets, we observed 118 stars, which were selected from the Hipparcos catalogue (ESA 1997) mainly based on the criterion of $V < 8.5$, $0.62 \lesssim B-V \lesssim 0.67$, and $4.5 \lesssim M_V \lesssim 5.1$[3]. This field of search, centered on the solar values of $(B-V)_\odot = 0.65$ and $(M_V)_\odot = 4.82$ (Cox 1999), was selected by considering the possible uncertainties (with a sufficient margin) of $B-V$ and M_V; i.e., a few hundredths mag for the former (cf. the note in the last paragraph of Sect. 3.2) and a few tenths mag for the latter (ambiguities due to parallax errors are typically ∼0.1–0.2 mag; in addition, other uncertainies such as the interstellar extinction or Lutz-Kelker correction may also have some minor contribution). The positions of the 118 targets on the HR diagram are depicted in Fig. 1.

The reduction of the spectra (bias subtraction, flat-fielding, scattered-light subtraction, spectrum extraction, wavelength calibration, and continuum normalization) was performed by using the "echelle" package of the software IRAF[4] in a standard manner. The stellar radial velocities were then determined by the cross-correlation method ("fxcor" task of IRAF) applied to the

[3] Since the effect of interstellar reddening/extinction was taken into account with the help of Arenou et al.'s (1992) tables, some stars are slightly redder than this criterion in terms of the apparent $B-V$. Besides, we intentionally included all of the top-ten solar analogs reported by Soubiran & Triaud (2004) in our sample.

[4] IRAF is distributed by the National Optical Astronomy Observatories, which is operated by the Association of Universities for Research in Astronomy, Inc. under cooperative agreement with the National Science Foundation.

Table 1. Basic observational data of 118 program stars.

HIP	HD	Sp.	$B-V$	V	π	σ/π	M_V	Date	$\langle S/N \rangle$	V_r
1499	1461	G0V	0.674	6.47	42.67	0.02	4.62	2005-09-28	140	−10.4
1598	1562	G0	0.640	6.97	40.25	0.02	4.99	2005-09-30	200	+14.9
1803	1835	G3V	0.659	6.39	49.05	0.02	4.84	2005-09-29	210	−2.6
4290	5294	G5	0.652	7.41	33.92	0.03	5.06	2005-09-26	180	−8.5
5176	6512	G0	0.656	8.15	20.84	0.05	4.74	2005-11-25	130	+10.1
6405	8262	G3V	0.627	6.96	39.07	0.02	4.92	2005-09-28	160	+5.5
6455	8406	G5V	0.656	7.92	27.00	0.04	5.08	2005-09-29	140	−8.0
7244	9472	G0	0.666	7.63	30.13	0.03	5.02	2005-09-28	150	+11.4
7585	9986	G5V	0.648	6.77	38.86	0.02	4.72	2005-09-26	250	−21.3
7902	10145	G5V	0.691	7.70	27.28	0.04	4.88	2005-11-24	160	+17.5
7918	10307	G2V	0.618	4.96	79.09	0.01	4.45	2005-09-26	390	+4.7
8486	11131	G0	0.654	6.72	43.47	0.10	4.91	2005-09-29	180	−4.9
9172	11926	G5	0.661	7.57	31.98	0.05	5.09	2005-11-24	160	−14.9
9349	12264	G5V	0.660	7.99	22.80	0.05	4.78	2005-09-29	130	+19.3
9519	12484	F8	0.649	8.18	21.24	0.06	4.82	2005-11-25	120	+4.5
9829	12846	G2V	0.662	6.89	43.14	0.02	5.06	2005-09-28	160	−4.8
10321	13507	G0	0.672	7.19	38.12	0.02	5.10	2005-09-28	190	+5.9
11728	15632	G0	0.666	8.03	23.90	0.05	4.92	2005-11-25	140	+4.5
12067	15851	G3V	0.696	8.42	20.28	0.05	4.96	2006-02-18	90	+9.7
14614	19518	G8V	0.642	7.85	24.44	0.04	4.79	2005-09-29	150	−27.5
14623	19632	G3/G5V	0.678	7.29	33.14	0.03	4.89	2005-09-26	90	+40.9
15062	20065	G5	0.624	8.12	24.52	0.04	5.07	2005-11-30	130	−17.9
15442	20619	G0	0.655	7.05	40.52	0.02	5.09	2005-09-28	170	+22.4
16405	21774	G5	0.680	8.08	20.04	0.06	4.59	2005-11-29	120	−3.3
17336	23052	G0	0.659	7.07	38.75	0.03	5.01	2005-09-28	190	−15.2
18261	24552	G0	0.631	7.97	22.13	0.06	4.69	2005-09-29	140	+15.9
19793	26736	G3V	0.657	8.05	21.69	0.05	4.73	2005-11-27	120	+37.2
19911	26990	G0	0.661	7.50	28.69	0.04	4.79	2005-09-29	170	−15.4
19925	27063	G0	0.669	8.07	24.81	0.04	5.04	2005-11-30	140	−10.1
20441	27685	G4V	0.677	7.86	26.96	0.05	5.01	2005-09-26	110	+35.7
20719	28068	G1V	0.651	8.04	21.76	0.07	4.73	2005-11-27	150	+35.1
20741	28099	G8V	0.664	8.10	21.42	0.07	4.75	2005-11-27	140	+38.1
20752	28192	G0	0.629	8.06	19.51	0.05	4.51	2005-11-30	140	−4.5
21165	27757	G5	0.630	7.83	23.97	0.03	4.73	2005-11-24	140	+36.8
21172	28821	G0	0.683	7.61	27.05	0.04	4.77	2005-12-01	150	+37.2
22203	30246	G5	0.665	8.30	19.42	0.06	4.74	2005-12-01	90	+41.8
23530	31864	G0	0.660	7.63	31.76	0.03	5.14	2005-11-24	180	−26.2
25002	35041	G6V	0.636	7.68	26.89	0.04	4.83	2005-12-01	90	−4.5
25414	35073	G5	0.700	8.35	20.64	0.05	4.92	2005-12-02	110	+1.8
25670	36152	G5V	0.657	8.27	21.35	0.05	4.92	2005-12-02	110	−9.6
26381	37124	G4IV-V	0.667	7.68	30.08	0.04	5.07	2005-11-24	180	−23.4
27435	38858	G4V	0.639	5.97	64.25	0.02	5.01	2005-09-29	240	+31.2
29432	42618	G4V	0.642	6.85	43.26	0.02	5.03	2005-11-24	160	−53.8
31965	47309	G0	0.672	7.60	23.57	0.04	4.46	2005-11-25	210	+27.4
32673	49178	G0	0.677	8.07	23.06	0.05	4.88	2005-11-25	160	+33.5
33932	49985	G0	0.627	8.31	20.88	0.04	4.91	2005-12-02	90	−12.3
35185	56202	G5	0.641	8.42	18.99	0.06	4.81	2006-02-17	90	+21.5
35265	56124	G0	0.631	6.93	36.50	0.03	4.74	2005-11-25	210	+22.2
36512	59711	G5V	0.637	7.73	27.36	0.03	4.92	2005-11-30	180	+7.9
38647	64324	G0	0.659	7.78	28.33	0.04	5.04	2005-11-30	150	+16.8
38747	64942	G5	0.671	8.37	20.69	0.06	4.95	2005-11-30	130	−8.5
38853	65080	G0	0.638	8.21	18.57	0.07	4.55	2005-11-29	100	−8.6
39506	66573	G0	0.632	7.26	33.88	0.03	4.91	2005-11-27	170	−44.7
39822	66171	G2V	0.621	8.18	21.15	0.04	4.81	2005-12-02	100	+36.0
40118	68017	G4V	0.679	6.78	46.05	0.02	5.10	2005-11-26	160	+29.3
40133	68168	G0	0.667	7.34	29.45	0.03	4.69	2005-11-29	150	+8.8
41184	70516	G0	0.652	7.71	27.10	0.08	4.87	2005-12-01	140	+8.0
41484	71148	G5V	0.624	6.32	45.89	0.02	4.63	2005-11-26	130	+8.1
41526	71227	G0V	0.639	7.98	22.29	0.05	4.72	2005-12-01	110	−1.2
42333	73350	G0	0.655	6.74	42.32	0.02	4.87	2005-11-26	150	+35.1
42575	73393	G3V	0.675	8.00	23.81	0.04	4.88	2005-12-01	110	+35.1
43297	75302	G0	0.689	7.45	33.50	0.03	5.08	2005-11-30	150	+9.9
43557	75767	G0	0.640	6.57	41.42	0.03	4.66	2005-11-26	210	+17.1
43726	76151	G3V	0.661	6.01	58.50	0.02	4.85	2005-11-27	210	+31.6
44324	77006	G5	0.651	7.93	23.23	0.04	4.76	2005-12-01	110	+4.4

Table 1. continued.

HIP	HD	Sp.	$B-V$	V	π	σ/π	M_V	Date	$\langle S/N \rangle$	V_r
44997	78660	G5	0.665	8.34	19.93	0.06	4.84	2006-04-17	90	−12.5
45325	79282	G5	0.654	8.30	17.61	0.06	4.53	2006-02-17	100	+3.7
46903	82460	G0	0.670	8.40	21.31	0.05	5.04	2006-02-18	100	+9.3
49580	87680	G2V	0.670	7.96	25.50	0.04	4.99	2005-12-02	100	−27.1
49586	87666	K0	0.664	8.15	20.83	0.05	4.74	2006-04-17	80	+29.6
49728	88084	G5V	0.649	7.52	28.37	0.03	4.78	2006-04-16	130	−24.0
49756	88072	G0	0.647	7.55	26.96	0.04	4.70	2006-04-16	140	−18.2
50505	89269	G5	0.653	6.66	48.45	0.02	5.09	2005-11-29	150	−7.7
51178	90494	F8	0.632	8.39	20.87	0.05	4.99	2006-04-16	110	+1.5
53721	95128	G0V	0.624	5.03	71.04	0.01	4.29	2005-11-29	260	+10.9
54375	96497	G1V	0.645	8.22	18.94	0.09	4.61	2006-04-17	90	−0.8
55459	98618	G5V	0.642	7.65	25.82	0.03	4.71	2006-04-16	150	+6.8
55868	99505	G5	0.630	7.59	30.76	0.04	5.03	2006-02-17	130	−0.1
59589	106210	G3V	0.667	7.57	29.50	0.03	4.92	2006-02-18	90	−24.9
59610	106252	G0	0.635	7.41	26.71	0.03	4.54	2006-02-19	130	+15.3
62175	110869	G5V	0.662	8.01	22.10	0.04	4.73	2006-04-16	100	−9.4
62816	111938	G0	0.632	8.48	18.78	0.05	4.85	2006-04-16	100	−11.7
63048	112257	G2V	0.665	7.80	23.84	0.04	4.69	2006-04-17	110	−40.0
63636	113319	G8IV	0.655	7.51	31.86	0.03	5.03	2006-02-17	130	+6.0
64150	114174	G5IV	0.667	6.78	38.07	0.02	4.68	2006-02-17	160	+24.2
64747	115349	G2V	0.640	8.29	22.39	0.04	5.04	2006-04-16	110	−47.0
70319	126053	G1V	0.639	6.25	56.82	0.02	5.02	2006-02-16	200	−19.5
72604	131042	G5	0.643	7.50	26.79	0.03	4.64	2006-02-18	110	−27.2
75676	138004	G5	0.676	7.48	31.10	0.02	4.94	2006-04-16	130	−8.7
76114	138573	G5IV-V	0.656	7.22	32.35	0.03	4.77	2006-02-17	150	−36.1
77749	142072	G5V	0.670	7.85	24.07	0.04	4.76	2006-04-17	100	−25.2
78217	144061	G5	0.654	7.26	34.35	0.03	4.94	2006-04-17	120	−9.0
79672	146233	G1V	0.652	5.49	71.30	0.01	4.76	2006-04-17	210	+11.2
85042	157347	G5IV	0.680	6.28	51.39	0.02	4.83	2005-09-26	220	−36.1
85810	159222	G5V	0.639	6.52	42.20	0.01	4.65	2005-09-28	220	−51.6
88194	164595	G2V	0.635	7.07	34.57	0.02	4.76	2005-09-29	200	+1.9
88945	166435	G0	0.633	6.84	39.62	0.02	4.83	2005-09-30	190	−14.6
89282	167389	F8	0.649	7.38	29.91	0.02	4.76	2005-09-30	150	−5.6
89474	168009	G2V	0.641	6.30	44.08	0.01	4.52	2005-09-30	180	−64.7
89912	168874	G2IV	0.636	6.99	33.99	0.02	4.65	2005-09-30	160	−20.2
90004	168746	G5	0.713	7.95	23.19	0.04	4.78	2005-09-26	90	−25.8
91287	171665	G5V	0.687	7.43	33.17	0.03	5.03	2005-09-29	130	−23.6
96184	184403	G0	0.654	7.81	22.52	0.05	4.57	2005-09-30	130	−27.2
96395	185414	G0	0.636	6.73	41.24	0.01	4.81	2005-09-28	160	−15.9
96402	184768	G5	0.675	7.55	25.56	0.04	4.59	2005-09-29	120	−13.5
96901	186427	G5V	0.661	6.25	46.70	0.01	4.60	2006-04-17	140	−28.3
96948	186104	G0	0.664	7.64	24.81	0.04	4.61	2005-09-29	160	−61.4
97420	187237	G2III	0.660	6.87	38.44	0.02	4.79	2005-09-28	210	−33.1
98921	190771	G5IV	0.654	6.18	52.99	0.01	4.80	2005-09-26	150	−26.2
100963	195034	G5	0.642	7.09	35.41	0.02	4.84	2005-09-28	230	−1.0
104075	200746	G5	0.654	7.97	22.57	0.13	4.74	2005-09-29	150	+14.7
109110	209779	G0	0.674	7.57	28.16	0.04	4.82	2005-09-28	140	−6.7
110205	211786	G5	0.666	7.98	23.88	0.04	4.87	2005-09-28	160	+21.6
112504	215696	G5V	0.684	7.35	29.51	0.05	4.70	2005-09-30	140	−30.7
113579	217343	G3V	0.655	7.47	31.22	0.03	4.94	2005-09-30	140	+6.4
113989	218209	G6V	0.646	7.49	33.65	0.02	5.12	2005-09-26	160	−16.3
115715	220821	G0	0.644	7.36	28.53	0.04	4.64	2005-09-26	180	−3.2
116613	222143	G5	0.665	6.58	43.26	0.02	4.76	2006-02-17	140	−0.4

Note. The basic stellar data in the first seven columns (HIP number, HD number, spectral type, $B-V$ color, V magnitude, parallax in milliarcsecond and its relative error) were taken from the Hipparcos catalog (ESA 1997), while M_V was derived from V and π. The last three columns give the information of our spectroscopic data adopted in this study (observation date, mean *S/N*, and the heliocentric radial velocity in km s^{-1}).

spectrum portion of 6050–6160 Å, and were further converted into the heliocentric scale ("dopcor" task).

The list of our program stars is presented in Table 1, where their fundamental quantities taken from the Hipparcos catalogue are also given. The mean *S/N* ratios given in this table were computed as $\langle S/N \rangle \equiv (4.2 \times \langle count \rangle)^{1/2}$, where $\langle count \rangle$ is the mean ADU count evaluated by "imstatistics" task of IRAF and 4.2 e$^-$/ADU is the gain factor. Since this is a rough estimate for the mean *S/N*, the actual values are dependent on the location within the echelle order (i.e., higher/lower in the center/edge of the order). Unfortunately, these $\langle S/N \rangle$ values are typically ∼100–200 and are not satisfactorily high for spectroscopic analyses, since we had to restrict the total exposure time for a star to $\lesssim$1–2 h at most, forced by the necessity of observing a large

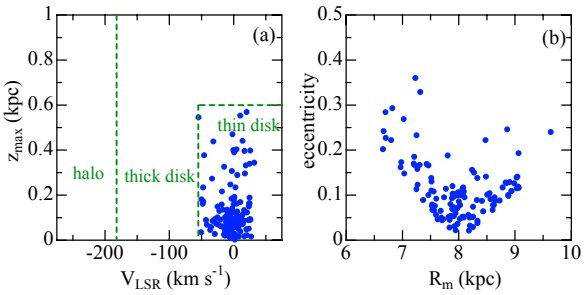

Fig. 2. a) Correlation diagram between z_{max} (maximum separation from the galactic plane) and V_{LSR} (rotation velocity component relative to LSR), which may be used to classify the stellar population (the halo/thick-disk/thin-disk boundaries are also shown by dashed lines according to Ibukiyama & Arimoto 2002). **b)** e (orbital eccentricity) plotted against R_m (mean galactocentric radius).

number of (7–)8 mag stars (which was severe requirement for high-dispersion spectroscopic observations with the 188 cm telescope at OAO).

We also examined the kinematic properties of each star by computing the orbital motion within the galactic gravitational potential based on the positional and proper-motion data (taken from the Hipparcos catalog) along with the radial-velocity data (measured by us), following the procedure described in Sect. 2.2 of Takeda (2007, herein referred to as Paper IV). While the input data and the solutions of the resulting kinematic parameters are given in (electronic) Table 2, Figs. 2a,b show the correlations of z_{max} (maximum separation from the galactic plane) vs. V_{LSR} (rotation velocity component relative to LSR) and e (orbital eccentricity) vs. R_m (mean galactocentric radius). We can see from Fig. 2a that all our program stars belong to the normal thin-disk population, according to Ibukiyama & Arimoto's (2002) classification criteria.

3. Stellar parameters

3.1. Atmospheric parameters

A stellar atmosphere is characterized by four parameters: the effective temperature (T_{eff}), the surface gravity ($\log g$), the microturbulent velocity dispersion (v_t), and the metallicity usually represented by the Fe abundance relative to the Sun ([Fe/H]). These have to be established, in order to construct an atmospheric model for a star and simulate theoretical spectra (e.g., for elemental abundance determinations).

We determined these four atmospheric parameters from the measured equivalent widths of Fe I and Fe II lines based on the computational procedure described in Takeda et al. (2002), which establishes the best solutions of these parameters satisfying the conditions of excitation/ionization equilibria and curve-of-growth matching, where we followed the two consecutive steps as described below.

3.1.1. Standard solutions

First, we obtained the "absolute" values of these parameters for our 118 program stars (plus the Sun), following the procedures adopted by Takeda et al. (2005b, hereinafter referred to as Paper I). See Sects. 2 and 3 therein for the description of the equivalent-width measurement for the usable Fe I and Fe II lines[5] and the computational procedure (i.e., an application of the TGVIT program). We call such established absolute parameters, T_{eff}^{std}, $\log g^{std}$, v_t^{std}, and $\{Fe/H\}^{std}(\equiv A_{Fe}^{std} - 7.50)$, the "standard" solutions[6]. The adopted atomic data, the measured equivalent widths, and the Fe abundances for each of the used lines (corresponding to the final parameter solutions) are presented in (electronic) Table 3, while the results of T_{eff}^{std}, $\log g^{std}$, v_t^{std}, and $\{Fe/H\}^{std}$ are given in (electronic) Table 4. Note that we obtained 5761.0 K, 4.435, 1.00 km s^{-1}, and −0.007 for the solar atmospheric parameters.

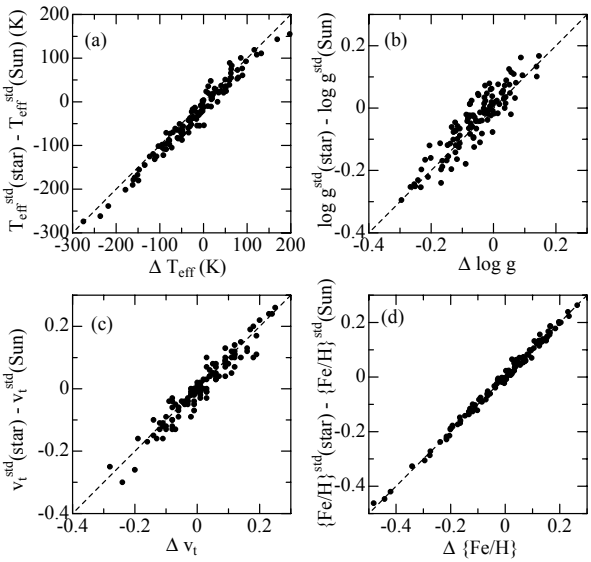

Fig. 3. Correlation of the star−Sun differences of atmospheric parameters derived by two different approaches: the simple differences of "standard" parameters obtained with the conventional spectroscopic method (Takeda et al. 2002; Paper I) on the one hand (ordinate), and those directly obtained by the complete differential method (Paper III) on the other (abscissa). **a)** T_{eff}, **b)** $\log g$, **c)** v_t, and **d)** {Fe/H}.

3.1.2. Differential solutions

Then, given the solutions of standard parameters, we further applied the technique described in Takeda (2005, hereinafter Paper III), which we may call the method of "complete differential analysis" (i.e., all parameters are differentially treated, where errors in the gf values or imperfections in the model atmosphere are cancelled), to any 118 (star−Sun) pair to establish the four "differential" parameters ΔT_{eff}, $\Delta \log g$, Δv_t, and $\Delta\{Fe/H\}$, where Δ means the star−Sun difference of the parameter[7]. The results are given also in Table 4.

The correlations betwen the simple differences of the standard parameters (p^{std}(star)−p^{std}(Sun)) and the solutions of differential parameters (Δp), where p is any of T_{eff}, $\log g$, v_t, and {Fe/H}, are shown in Fig. 3. As can be recognized from this figure, both are mostly in good agreement. Although we expected a quantitatively more appreciable change (with a markedly improved precision) in the differential solution compared to the standard one as was experienced in Paper II (see

[5] We used the 5600–6800 Å region of the Moon spectrum included in the database of Takeda et al. (2005a) to evaluate the solar equivalent widths.

[6] A denotes the logarithmic abundance in the usual normalization of $A_H = 12.00$.

[7] Note that $\Delta\{Fe/H\}$ is equivalent to [Fe/H] ($\equiv A_{Fe}^{star} - A_{Fe}^{Sun}$) according to the definition of {Fe/H} ($\equiv A_{Fe} - 7.50$).

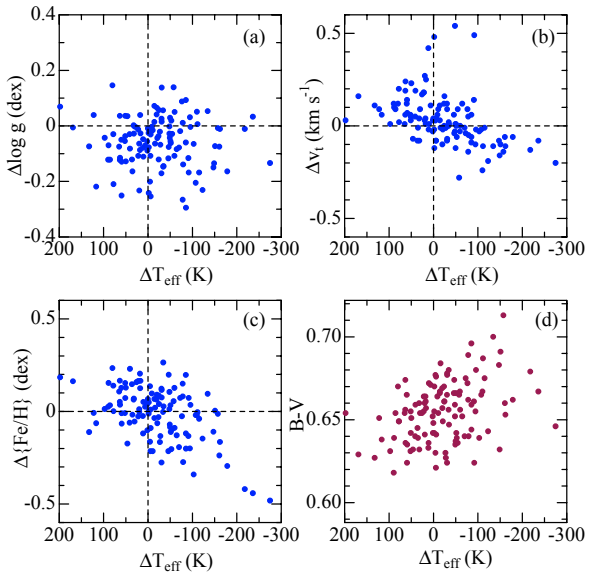

Fig. 4. Mutual correlation of star−Sun parameter differences obtained by the complete differential method: **a)** $\Delta \log g$ vs. $\Delta T_{\rm eff}$, **b)** $\Delta v_{\rm t}$ vs. $\Delta T_{\rm eff}$, and **c)** Δ {Fe/H} vs. $\Delta T_{\rm eff}$. The relation between $B-V$ and $\Delta T_{\rm eff}$ is shown in panel **d)**.

Figs. 2a–d therein, which are equivalent to Figs. 3a–d in this paper)[8], it is certain that the precision in Δp has been improved compared to $p^{\rm std}$(star)$-p^{\rm std}$(Sun). Actually, the mean statistical errors (averaged over all stars; individual errors vary from star to star typically by a factor of $\lesssim$2–3 from these means) for the four parameters evaluated in a manner described in Sect. 5.2 of Takeda et al. (2002) are 17 K, 0.04 dex, 0.09 km s^{-1}, and 0.02 dex for the former, which are slightly better than those of 20 K, 0.05 dex, 0.10 km s^{-1}, and 0.02 dex for the latter. Therefore, we will refer to the Δ values as the atmospheric parameters in the rest of this paper whenever possible (e.g., use of $\Delta T_{\rm eff}$ when discussing the $T_{\rm eff}$-dependence of $A_{\rm Li}$).

3.2. Distributions and mutual correlations

The resulting solutions of $\Delta \log g$, $\Delta v_{\rm t}$, and Δ\{Fe/H\} are plotted against $\Delta T_{\rm eff}$ in Fig. 4, where the correlation between $B-V$ and $\Delta T_{\rm eff}$ is also shown.

While we see from Fig. 4a that the distribution of $\Delta \log g$ is slightly biased toward a lower gravity, it is not clear whether this is meaningful, since our spectroscopic gravity may have been somewhat underestimated for those stars in the low-gravity region (Sect. 3.3).

Figure 4b shows that $v_{\rm t}$ tends to decrease toward a lower $T_{\rm eff}$ with a gradient of $\sim$−0.1 km s^{-1}/100 K, which is consistent with the global trend established in Fig. 2b of Paper I. That this tendency is recognizible even in a narrow $T_{\rm eff}$-interval of $\sim$200 K may suggest that the precision in our $\Delta T_{\rm eff}$ is satisfactorily high (with a resolution of $\sim$20 K).

While the metallicities of our program stars are distributed mostly around the solar value (Fig. 4c), several stars with appreciably low $\Delta T_{\rm eff}$ as well as low Δ\{Fe/H\} are included, which are located at the lower-right corner of this figure. This may be interpreted as due to our solar-analog selection process based on $B-V$ colors; i.e., unwanted low-$T_{\rm eff}$, low-metal stars may happen to be inadequately picked up because they may accidentally have near-solar $B-V$ values (i.e., both effects of reddening and blueing tend to cancel each other).

While the $B-V$ vs. $\Delta T_{\rm eff}$ relation shown in Fig. 4d reveals that the correlation is rather poor, this is primarily due to the fact that stars with a variety of metallicities are mixed together. Since the relation $\delta(B-V) \sim 0.1\delta$[Fe/H] approximately holds (e.g., Alonso et al. 1996), a scatter in [Fe/H] by a few tenths dex causes a blurring of $B-V$ by a few hundredths mag, which ecceeds the typical intrinsic $B-V$ error of $\sim$0.01 mag (the average for our sample stars). If the metallicity is known in advance or if a color index less affected by the metallicity (e.g., $V-K$) is used, this kind of uncertainty may be reduced. Yet, since even only the intrinsic error of $\delta(B-V) \sim 0.01$ mag itself leads to an ambiguity of $\sim$30–40 K in $T_{\rm eff}$ for solar-type stars (Alonso et al. 1996), color-based $T_{\rm eff}$ determinations must have less precision than the spectroscopic approach.

3.3. Age and mass

The stellar age (*age*) and mass (M) were evaluated by comparing the position on the $\log L$ vs. $\log T_{\rm eff}$ diagram (theoretical HR diagram) with the theoretically stellar evolutionary tracks[9] in the same manner as in described Paper IV (cf. Sect. 2.1 therein). The theoretical tracks used here were those of Girardi et al. (2000) computed "with overshooting" for different metallicities (z) as shown in Figs. 5a,b, where our program stars are also overplotted.

By using such determined M, we computed the theoretical $\log g_{TLM}$ (with the help of already known $T_{\rm eff}^{\rm std}$ and Hipparcos-based L), which is compared with the spectroscopic $\log g^{\rm std}$ in Fig. 5c. We see from this figure that $\log g^{\rm std}$ appears to be somewhat lower than $\log g_{TLM}$ at the lower gravity side ($\log g \sim$ 4.2–4.3). Since such a tendency was not observed in the study of general field stars in Paper I (cf. Fig. 5 therein), $\log g^{\rm std}$ for those stars may have been systematically understimated by $\sim$0.1–0.2 dex (possibly due to insufficient data quality/quantity), which we have to bear in mind; for example, in interpreting Fig. 4a.

As in Paper IV, the reliability of the *age* solution was classified into three groups according to δ, the difference between $\log$ *age* (determined by interpolating *tracks*: adopted here) and $\log(age)_{\rm iso}$ (determined in a superficially different manner by interpolating *isochrones*), as $|\delta| < 0.1 \cdots$ group A (reliable), $0.1 < |\delta| < 0.3 \cdots$ group B (tolerable), and $0.3 < |\delta| \cdots$ group C (unreliable). The correlation between the resulting *age* and M values is shown in Fig. 5d, where the reliability of *age* is discerned by the difference in symbols and the error bars were estimated from uncertainties in $\log L$, $\log T_{\rm eff}$, and $\log z$ as was done Paper IV (cf. Sect. 2.1 therein for more details). We can see from this figure that *age* and M of our solar-analog sample stars tend to be anti-correlated with each other.

[8] This fact (the improvement in the parameter precision is quantitatively inconspicuous) may be interpreted as follows. Compared to the analysis in Paper II, the precision of *EW* measurement is lower in this study (because of insufficient *S/N* ratios of the spectra) and the number of the lines used are about half as small. Therefore, precisions in the solutions are presumably determined by errors in the input observational data (influencing equally both types of analyses), and not by errors due to gf values or spectrum modeling (from which differential solutions are almost free, unlike the standard solutions). Accordingly, the merit of the differential solution may not have been much demonstrated.

[9] That is, the *age* and M, to which we refer here, are the $age_{\rm trk}$ and $M_{\rm trk}$ defined in Paper IV.

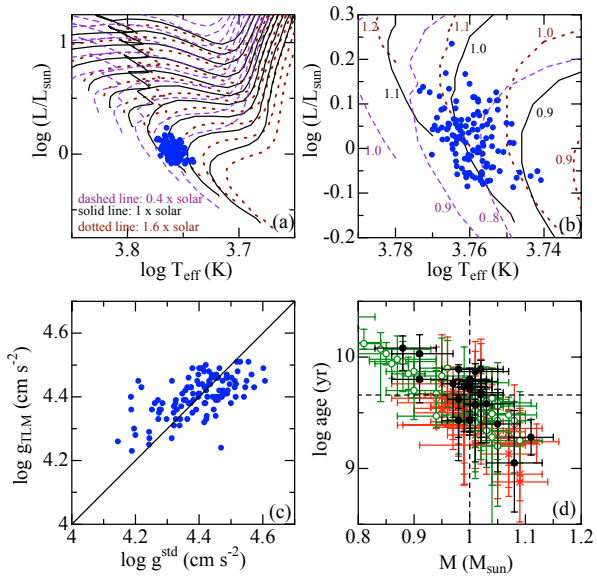

Fig. 5. a) Our 118 program stars (symbols) plotted on the theoretical HR diagram, where the theoretical evolutionary tracks of Girardi et al. (2000) are also drawn for 10 mass values ranging from 0.8 to 1.7 $M_{\rm sun}$ with a step of 0.1 $M_{\rm sun}$ for three different metallicities: $z = 0.008$ (0.4 × solar, dashed line), $z = 0.019$ (1× solar, solid line), and $z = 0.030$ (1.6 × solar, dotted line). **b)** Scale-up of panel **a)**. **c)** Comparison of the spectroscopically determined surface gravities ($\log g^{\rm std}$) with those derived from the stellar fundamental quantities of $T_{\rm eff}$, L, and M ($\log g_{TLM}$). **d)** Relation between the mass and age derived from the evolutionary tracks. The symbol type discriminates the reliability of *age* (cf. Sect. 3.3): filled circles (good, class A), open circles (moderate, class B), and crosses (poor, class C). See also Sect. 3.3 for the description of the error bars.

The complete results of these M and *age* determinations, along with the related basic stellar quantities, are given in Table 4.

4. Abundance and broadening-width determinations

4.1. Model atmospheres

As to the atmospheric parameters for constructing the model atmospheres of 118 target stars, we adopted the standard solutions[10] derived in Sect. 3.1.1 ($T_{\rm eff}^{\rm std}$, $\log g^{\rm std}$, $v_{\rm t}^{\rm std}$, and $\{{\rm Fe/H}\}^{\rm std}$) as the $T_{\rm eff}$, $\log g$, $v_{\rm t}$, and [Fe/H] to be assigned to each star. The atmospheric models for individual stars were generated by interpolating Kurucz's (1993) grid of ATLAS9 model atmospheres in terms of $T_{\rm eff}$, $\log g$, and [Fe/H] (assumed to represent the model metallicity $[X]$).

4.2. Spectrum fitting of the 6080–6089 region

Given the atmospheric models, we first applied the automatic spectrum-fitting technique (Takeda 1995a) to the 6080–6089 Å region, in order to determine the abundances of Si, Ti, V, Fe, Co, and Ni ($A_{\rm Si}^{6085}$, $A_{\rm Ti}^{6085}$, $A_{\rm V}^{6085}$, $A_{\rm Fe}^{6085}$, $A_{\rm Co}^{6085}$, and $A_{\rm Ni}^{6085}$) and the macrobroadening parameter ($v_{\rm M}$; e-folding half-width of the Gaussian macrobroadening function, $f_{\rm M}(v) \propto \exp[(-v/v_{\rm M})^2]$) for our 118 program stars and the Sun (Moon). See Sect. 3.2.2 of Takeda et al. (2001) for more details of this procedure including the adopted gf values.

Since such derived $v_{\rm M}$ includes the contribution of instrumental broadening corresponding to the resolving power of $R \sim 70\,000$ (Sect. 2), this effect (Gaussian $FWHM$ of $\sim 3 \times 10^5/70\,000 \sim 4.29$ km s^{-1}, which corresponds to the e-folding half-width of $4.29/(2\sqrt{\ln 2}) \sim 2.57$ km s^{-1}) was subtracted to obtain the atmospheric macrobroadening parameter $v_{\rm r+m}$, which is defined as $v_{\rm r+m} \equiv \sqrt{v_{\rm M}^2 - 2.57^2}$ and represents the combined effects of projected rotational velocity ($v_{\rm e} \sin i$) and macroturbulence velocity dispersion ($v_{\rm mt}$); see, e.g., Gray (2005).

The finally established solutions of $A_{\rm Ti}^{6085}$, $A_{\rm V}^{6085}$, $A_{\rm Fe}^{6085}$, $A_{\rm Co}^{6085}$, $A_{\rm Ni}^{6085}$, and $v_{\rm r+m}$ are given in (electronic) Table 5, and the theoretical spectra corresponding to the final best-fit solutions (along with the observed spectra) are shown in Fig. 6.

The resulting synthesis-based $[{\rm Fe/H}]^{6085}$ ($\equiv A_{\rm Fe}^{6085} - A_{\rm Fe,\odot}^{6085}$) are compared with the already determined equivalent-width based $[{\rm Fe/H}]^{\rm std}$ ($\equiv A_{\rm Fe}^{\rm std} - A_{\rm Fe,\odot}^{\rm std}$; Sect. 3.1.1) in Fig. 7a. While the former tends to be slightly lower than the latter by ~0.03 dex on average, we may regard that the agreement is mosly reasonable, considering the not-so-high quality of the spectra. The $[{\rm X/Fe}]^{6085}$ vs. $[{\rm Fe/H}]^{6085}$ relations for Si, Ti, V, Fe, Co, and Ni are plotted in Figs. 7b–f, from which we can confirm that the general tendency is similar to the results of Paper IV (cf. Fig. 10 therein).

4.3. Analysis of the Li 6708 line

We then determined the lithium abundances from the Li I resonance doublet at 6708 Å (or the upper limits if this line is too weak to be measurable) in the same manner as in Paper II, which should be consulted for detailed descriptions of this procedure consisting of three consecutive steps:

(i) automatic profile fitting (in LTE) to determine $A_{\rm Li}^{\rm LTE}$;
(ii) inversely synthesizing (in LTE) the Li 6708 line equivalent width (EW_{6708}) with $A_{\rm Li}^{\rm LTE}$ as given;
(iii) non-LTE analysis of EW_{6708} to obtain $A_{\rm Li}^{\rm NLTE}$;

In applying step (i) to each star, we carefully examined the spectrum feature of the Li I 6708 line, and classified individual cases into three groups:

- Group (a): the line has a sufficiently large strength and the resulting $A_{\rm Li}$ is fairly reliable.
- Group (b): a slight depression-like feature is barely observable (though not confidently) at the position of the line, and we managed to derive $A_{\rm Li}$, which however may suffer considerably large uncertainties.
- Group (x): we could not detect any sign of depression for the Li I 6708 line, and jumped to step (iii) with an estimated upper limit of EW_{6708}.

The resulting best-fit theoretical spectra (and the observed spectra) around this Li I 6708 region are shown in Fig. 8. The results of this analysis are presented in (electronic) Table 6, which constitute the basic data for our discussion about $A_{\rm Li}$ in the next section, where we will concentrate primarily on group-(a) stars.

Then, what about the errors in such established Li abundances? Regarding the precision in the resulting $A_{\rm Li}$, the same argument as given in Sect. 3.3 of Paper II holds for the error components caused by uncertainties in atmospheric parameters (i.e., well below $\lesssim$0.1 dex). Due to the algorithm of our automatic

[10] This is because standard solutions ($p^{\rm std}$) are absolute parameters, which can be directly/naturally applied to constructing model atmospheres. Of course, we could alternatively use differential solutions (Δp; cf. Sect. 3.1.2) by converting them to absolute values as $p_\odot + \Delta p$; however the results must be practically the same (cf. Fig. 3).

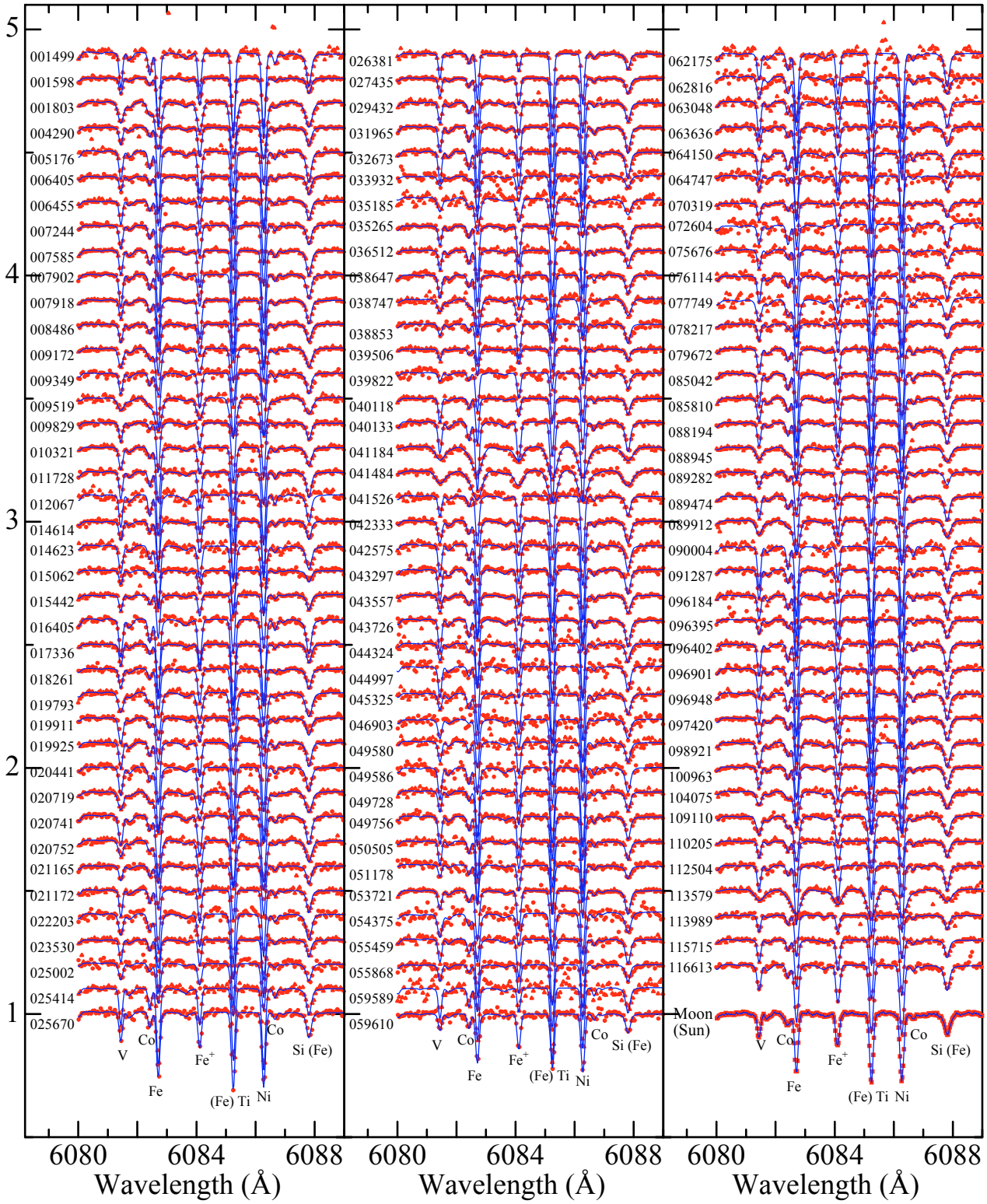

Fig. 6. Synthetic spectrum fitting analysis of the 6080–6089 Å region to determine the macrobroadening parameter as well as the abundances of Si, Ti, V, Fe, Co, and Ni. The best-fit theoretical spectra are shown by solid lines, while the observed data are plotted by symbols. A vertical offset of 0.1 is applied to each relative to the adjacent ones. Indicated on the left to the spectrum is the HIP number, while the case of Moon (Sun) is displayed at the lower-right of the figure.

profile-fitting method (Takeda 1995a) which does not require any information on the precise continuum level prior to analysis, errors caused by ambiguities in the continuum-placement are not relevant here. Meanwhile, errors in *EW*(Li I 6708) related to *S/N*-dependent photometric ambiguities are typically several mÅ as inferred from the upper limit values, which are also consistent to an order-of-magnitude with the estimations based on the relation suggested by Cayrel (1988). Considering that 10 mÅ $\lesssim$ *EW*(Li I 6708) $\lesssim$ 100 mÅ in most of our cases (cf. Table 6), we may consider that the error of this kind is again insignificant,

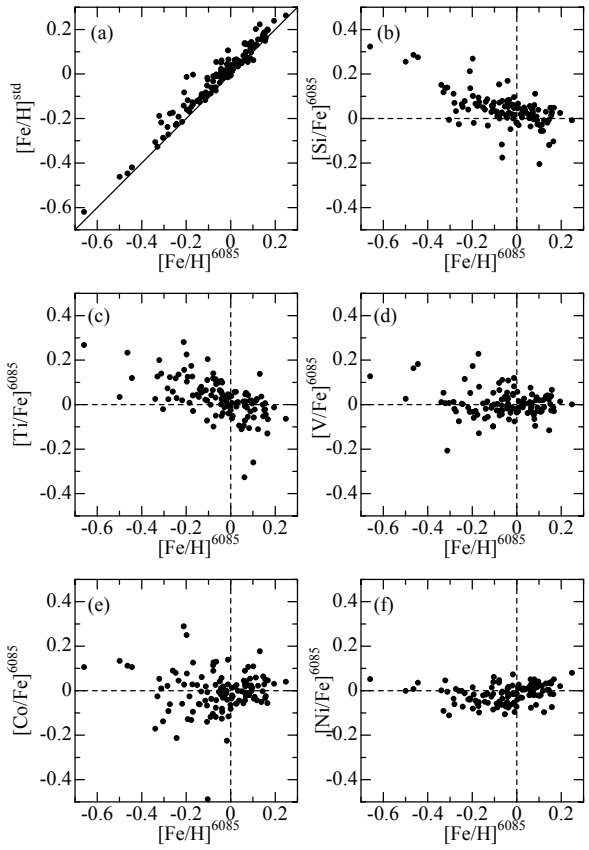

Fig. 7. Characteristics of the elemental abundances (A_X^{6085}, X = Si, Ti, V, Fe, Co, and Ni) derived from the 6080–6089 Å fitting. Note that $[X/H]^{6085} \equiv A_X^{6085}(\text{star}) - A_X^{6085}(\text{sun})$, and $[X/Fe]^{6085} \equiv [X/H]^{6085} - [Fe/H]^{6085}$. While panel **a)** depicts the correlation between $[Fe/H]^{6085}$ and $[Fe/H]^{std}$ (i.e., ordinate of Fig. 3d), panels **b)–f)** show the runs of $[X/Fe]^{6085}$ against $[Fe/H]^{6085}$ for Si, Ti, V, Fe, Co, and Ni, respectively.

except for the case near to the detection limit. Consequently, the general tendency of A_{Li} (ranging over ∼2 dex), to be discussed in Sect. 5, is hardly affected by errors involved in the abundance determination.

5. Discussion: Li abundance behaviors

5.1. General trend

The resulting Li abundances (A_{Li}) for our targets of 118 solar analogs are plotted against ΔT_{eff} in Fig. 9a, where three groups are distinguished by symbols and the solar abundance ($A_{Li,\odot}$ = 0.92; cf. Paper III) is also indicated. For comparison, we show the A_{Li} vs. T_{eff} relation for field stars in Fig. 9b (the same as Fig. 11b of Paper III), where the data for planet-host stars and non-planet-host stars were taken from Israelian et al. (2004) and Paper III, respectively.

Inspecting Fig. 9a, we can see that the distribution is roughly characterized by a triangle; i.e., a slanted boundary running from $A_{Li} \sim 3$ at $\Delta T_{eff} \sim +200$ K to $A_{Li} \sim 1$ at $\Delta T_{eff} \sim 0$ K (below which no stars exist), and a vertical boundary at $\Delta T_{eff} \sim -100$ K (lower than which the Li line becomes suddenly invisible).

At the lowest edge (nearly at the apex) of this triangle zone lies the Sun, which is apparently an outlier position among the considerably large dispersion (≳2 dex). Some (several to ∼10) Li-invisible stars of near-solar T_{eff}, for which only upper limits of A_{Li} could be estimated, may share the common property with the Sun. However, little can be said about whether the solar $A_{Li,\odot}$ (∼1) is the lowest possible limit in this region or if any of these associates have significantly lower A_{Li} than this, until the Li line of these stars is intensively investigated based on extremely high *S/N* (desirably $\gtrsim 10^3$) data. Anyhow, our Sun belongs to a minority group of Li-weak stars with respect to the surface lithum abundance.

Since only 5 planet-host stars (HIP 26381, HIP 53721, HIP 59610, HIP 90004, and HIP 96901) are included in our sample (and Li could not be detected for 3 of them), a statistically meaningful discussion on the effect of planets is difficult. Nevertheless, we see the trend argued in Paper III (cf. Fig. 9b) that A_{Li}'s of planet-host stars lie on the lower envelope at $T_{eff} \sim$ 5800–5900 K. Namely, HIP 53721 and HIP 59610 are both on the slantly-running lower boundary at $\Delta T_{eff} \sim 100$–0 K. Further, considering that $A_{Li} \sim 0.5$ was derived by King et al. (1997) for HIP 96901 (16 Cyg B) based on a very high *S/N* Keck spectrum and the Sun has $A_{Li,\odot} \sim 0.9$, all these four objects (three planet host stars and the Sun) are located on the boundary line of $A_{Li} \simeq 1 + 1\,(\Delta T_{eff}/100\text{ K})$. That is, as far as our sample is concerned, all relevant planet-host stars (including our Sun) are aligned on this boundary.

Besides, this boundary region appears to be separated by a narrow gap running parallel to it, which further makes us speculate that this elongated/isolated island might be a special zone occupied by stars with planets. Anyway, those relevant boundary-line still-non-planet-host stars (e.g., HIP 5176, HIP 7918, HIP 18261, HIP 20752, HIP 33932, HIP 38853, HIP 43557, HIP 44324, HIP 45325, HIP 55459, HIP 85810, HIP 96184, HIP 104075, and HIP 116613) may deserve particular attention, since they might someday turn out to harbor planets.

5.2. Role of each stellar parameter

To study the origin of these characteristics, we examine whether and how the distribution of A_{Li} depends upon several stellar parameters which are considered to be important; i.e., T_{eff}, *age*, [Fe/H], and v_{r+m}. Our discussion will be confined to the A_{Li} values of group (a) (reliably determined case; Sect. 4.3). As a prerequisite for this inspection, the mutual correlations of these key parameters are shown in Figs. 10a–d.

5.2.1. T_{eff}, age, and metallicity

It has been occasionally considered that A_{Li} in late-type stars may be a function of T_{eff}, *age*, and metallicity ([Fe/H]), since the depletion of Li is considered to be determined by the convection zone depth (i.e., the efficiency of envelope mixing), which depends on T_{eff} and [Fe/H] in the sense that convection penetrates deeper as T_{eff}/[Fe/H] becomes lower/higher, as well as by the elapsed time (*age*). Actually, however, it is almost certain that the situation is not so simple and some other (still unknown) parameter must play a significant role (see, e.g., Pasquini et al. 1994, 1997, for detailed discussions).

We show A_{Li}–T_{eff}–*age* and A_{Li}–T_{eff}–[Fe/H] relations in Figs. 11 and 12, respectively. Combining these with Figs. 9 and 10, we see:

– While the global trend of enhanced A_{Li} depletion at a lower T_{eff} is obvious over a wide T_{eff} span, it is not clear from these figures whether A_{Li} is sensitively affected by

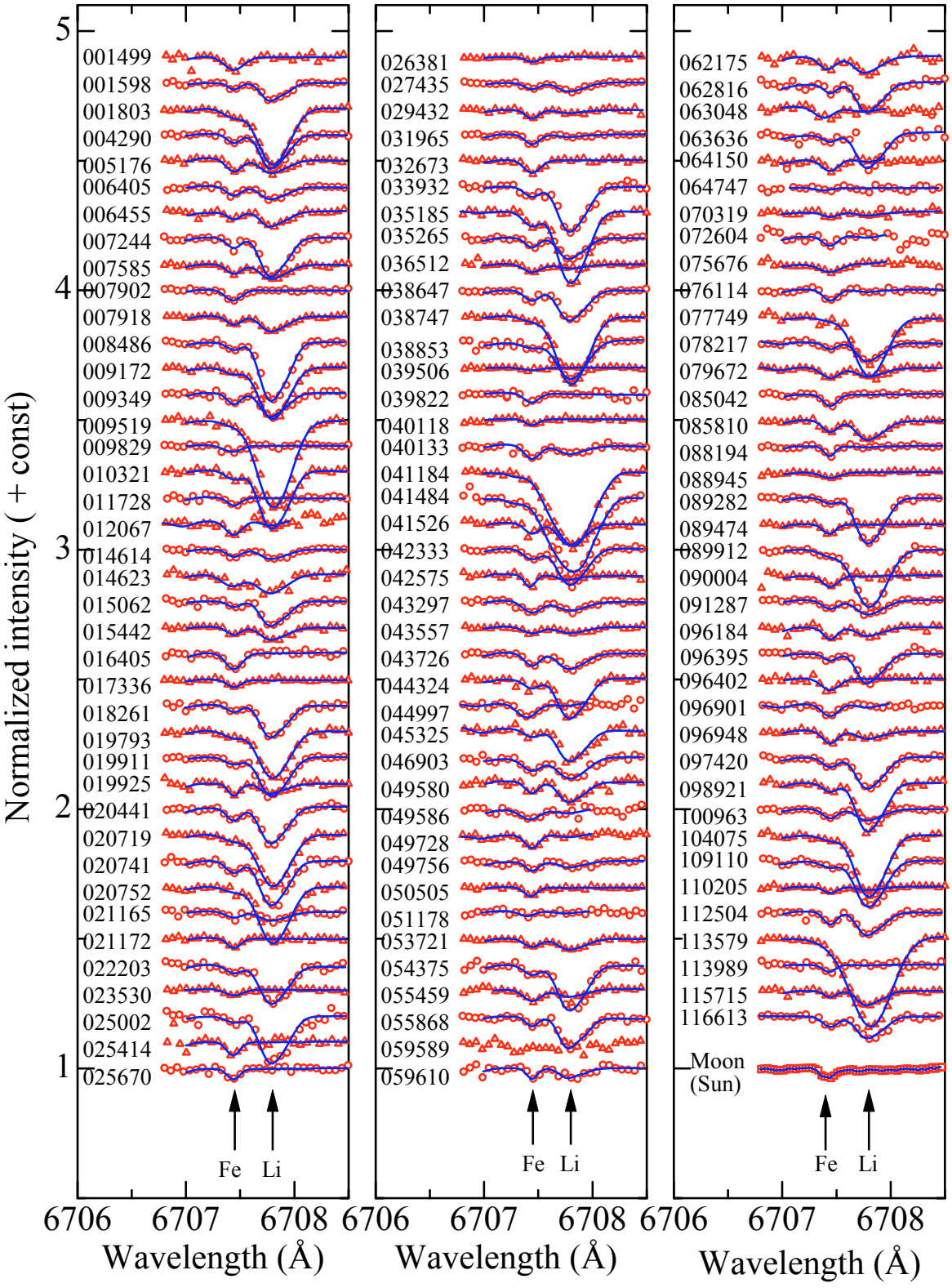

Fig. 8. Synthetic spectrum-fitting analysis of the Fe I+Li I line feature at the 6707–6708 Å region to determine the abundance of lithium. Otherwise, the same as in Fig. 6.

a slight change in $T_{\rm eff}$, because its dispersion at a given $T_{\rm eff}$ is too large[11].

– Figure 11b suggests a weak dependence of $A_{\rm Li}$ upon *age* as expected, although it is not very manifest.

[11] However, $A_{\rm Li}$ may be sensitive to $T_{\rm eff}$, since the results for the selected 26 solar-twin candidates having similar parameters (discussed in Appendix A) appear to imply such a decreasing trend (with a decrease in $\Delta T_{\rm eff}$) within a very narrow $T_{\rm eff}$ interval of only ~100 K (cf. Fig. A.1a).

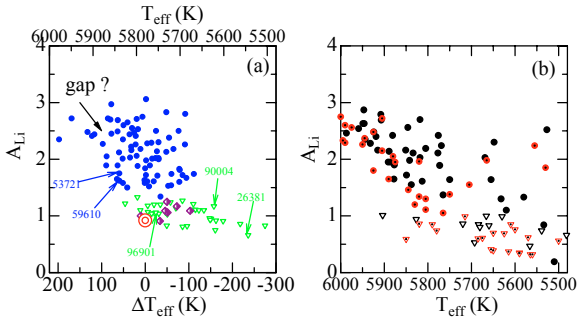

Fig. 9. a) $A_{\rm Li}$ vs. $\Delta T_{\rm eff}$ relation for the 118 solar analogs from our study. The filled circles, half-filled diamonds, and open downward triangles correspond to fairly reliable $A_{\rm Li}$ values (group (a)), rather uncertain $A_{\rm Li}$ values (group (b)), and upper limits (group (x), for which the Li line could not be detected), respectively. The large double-circle indicates the solar Li abundance. Five planet-harboring stars, included in our sample, are indicated by their HIP numbers. **b)** The $A_{\rm Li}$ vs. $T_{\rm eff}$ relation for field stars, where the data for planet-host stars (center-dotted symbols) and non-planet-host stars (simple symbols) were taken from Israelian et al. (2004) and Paper III, respectively. The downward triangles indicate the upper limits. This panel is a redrawn version of Fig. 11b in Paper III.

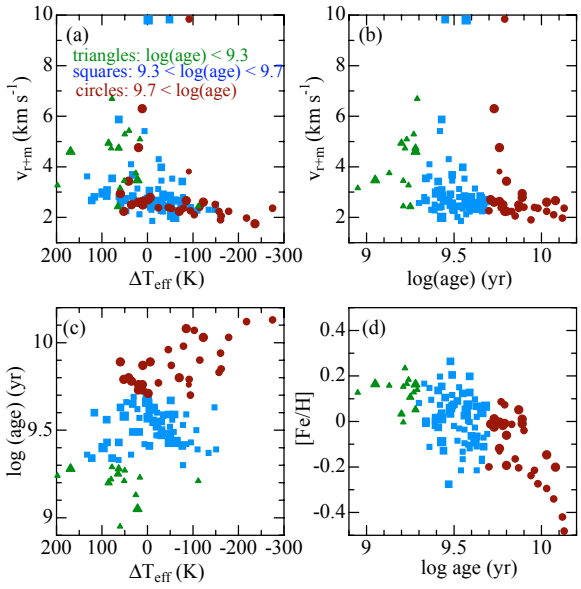

Fig. 10. Mutual correlations between the important parameters ($\Delta T_{\rm eff}$, $v_{\rm r+m}$, *age*, [Fe/H]) for all our 118 sample stars. The data points are grouped and expressed by different symbols according to the range of log *age* (yr), while the reliability of age-determination is indicated by the symbol size: large/middle/small symbol corresponds to reliability class of A(high)/B(moderate)/C(low), respectively. **a)** $v_{\rm r+m}$ vs. $\Delta T_{\rm eff}$, **b)** $v_{\rm r+m}$ vs. log *age*, **c)** log *age* vs. $\Delta T_{\rm eff}$, and **d)** [Fe/H] vs. log *age*.

– We see from Fig. 10c that a weak correlation exists between $T_{\rm eff}$ and *age*, which may (at least partly) be the reason for the non-detection of Li at $\Delta T_{\rm eff} \lesssim -100$ K (Fig. 9a) since they are comparatively old (~several to ten billions of years).
– According to Fig. 12b, a marginal [Fe/H]-dependence is observed in $A_{\rm Li}$. However, we do not consider this to be a real metallicity effect, since the trend (increase of $A_{\rm Li}$ with [Fe/H]) is the opposite to what is theoretically expected (decrease of $A_{\rm Li}$ with [Fe/H], since an enhanced metallicity would deepen the convection zone). Instead, this may be interpreted as due to the *age*-dependence of $A_{\rm Li}$, since [Fe/H] is weakly correlated with *age* (Fig. 10d)[12].
– In this connection, Domínguez Cerdeña et al.'s (2006) argument, that the low-Li tendency of planet-host stars may reflect a metallicity effect caused by deepened convection zone (owing to their metal-richness), seems unlikely, since we could not confirm such an $A_{\rm Li}$ vs. [Fe/H] anti-corelation expected from theory.

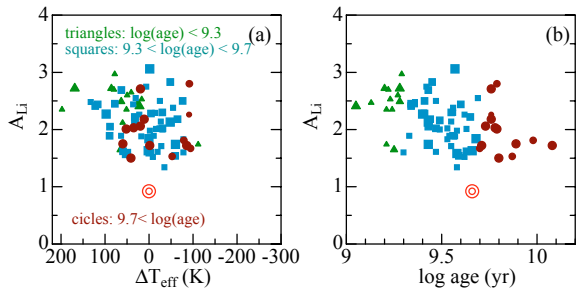

Fig. 11. Dependence of the lithium abundances upon *age* for the 76 stars of "group (a)" (i.e., for which $A_{\rm Li}$s were well determined). The *left panel* **a)** shows the $A_{\rm Li}$ vs. $\Delta T_{\rm eff}$ relation where the data points are grouped and expressed by different symbols according to the range of log *age* (with the *age*-reliability class indicated by the symbol size; cf. the caption of Fig. 10), while the *right panel* **b)** displays the $A_{\rm Li}$ vs. log *age* relation.

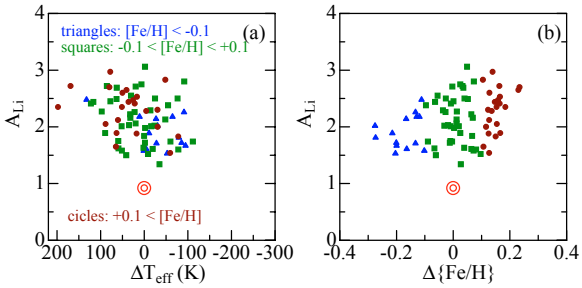

Fig. 12. Metallicity-dependence of the lithium abundances for the 76 stars of "group (a)" (i.e., for which $A_{\rm Li}$s were well determined). The *left panel* **a)** shows the $A_{\rm Li}$ vs. $\Delta T_{\rm eff}$ relation where the data points are grouped and expressed by different symbols according to the range of [Fe/H], while the *right panel* **b)** displays the $A_{\rm Li}$ vs. Δ[Fe/H] (≡[Fe/H]) relation.

5.2.2. Line-width dependence

As shown above, none of those three parameters ($T_{\rm eff}$, *age*, and metallicity) appears to be the key factor clarifying the origin of the considerable dispersion of $A_{\rm Li}$ in the homogeneous group of solar analog stars, even if they show rather loose (but meaningful) mutual correlations from a global point of view.

However, our analysis has suggested a promising parameter which appears to decisively influence the extent of $A_{\rm Li}$ for such stars of narrow parameter ranges; that is, the macrobroadening width ($v_{\rm r+m}$). Figure 13 shows the $v_{\rm r+m}$-dependence of $A_{\rm Li}$ in relation to its huge diversity in the $T_{\rm eff}$ vs. $A_{\rm Li}$ diagram. In addition, the results for the G-type stars in the Hyades cluster (obtained in the same manner as this study; Takeda et al., in preparation) are also plotted for comparison. As can be seen from Fig. 13b, $A_{\rm Li}$

[12] Similarly, since M (mass) is anticorrelated with *age* (cf. Fig. 5d), the *age*-dependence of $A_{\rm Li}$ further leads to the correlation between M and $A_{\rm Li}$, which is observed in F–G type field stars (e.g., Chen et al. 2001; Paper II).

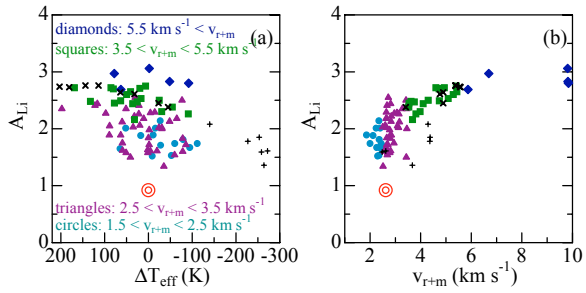

Fig. 13. Dependence of the lithium abundances upon v_{r+m} for the 76 stars of "group (a)" (i.e., for which A_{Li}s were well determined). The *left panel* **a)** shows the A_{Li} vs. ΔT_{eff} relation where the data points are grouped and expressed by different symbols according to the range of v_{r+m}, while the *right panel* **b)** displays the A_{Li} vs. v_{r+m} relation. In addition, the results for the 14 selected solar-analog G dwarfs (6000 K < T_{eff} < 5500 K) in the Hyades cluster, which were obtained in the same manner as this study (Takeda et al., in preparation), are overplotted by crosses for a comparison in both panels (stars higher or lower than T_{eff} of 5700 K are discriminated by St. Andrew's crosses [×] or Greek crosses [+], respectively).

has a significantly tight correlation with v_{r+m} (namely, A_{Li} becomes higher with an increase in v_{r+m}), which we may regard as evidence for its importance.

We can also recognize from Fig. 13b that the Hyades solar-analogs (*age* ~ 8×10^8 yr; cf. Dias et al. 2002) at +100 K $\gtrsim \Delta T_{eff} \gtrsim -100$ K closely follows this A_{Li} vs. v_{r+m} relation derived from our sample stars ($10^9 \lesssim$ *age* $\lesssim 10^{10}$ yr; cf. Fig. 10c) in spite of the considerable difference in *age* between these two groups. This indicates that *age* does not play any significant role in the diversity of A_{Li} in this narrow T_{eff} range[13]. Hence, we may conclude that A_{Li} is almost *age*-independent while strongly controled by v_{r+m} for those stars showing a large A_{Li} dispersion (at +100 K $\gtrsim \Delta T_{eff} \gtrsim -100$ K)[14].

Then, which of the rotation ($v_e \sin i$) and macroturbulence (v_{mt}) would contribute more dominantly to producing the A_{Li} vs. v_{r+m} relation, given that v_{r+m} (ranging from 2 km s^{-1} to 10 km s^{-1}) is actually a combination of these two effects? Although any confident statement can not be made unless they are separately determined (almost hopeless in the present case because of insufficient data quality), we can speculate that v_e (equatorial rotation velocity)[15] is the factor that affects A_{Li}, since such a considerable fluctuation of the macroturbulent velocity field[16] among similar solar-type stars is hard to imagine (given the fairly modest behavior of the microturbulence within 0.8 $\lesssim v_t \lesssim$ 1.2 km s^{-1}; cf. Fig. 4b). Namely, the star-to-star variation in $v_e \sin i$ may be the primary cause for the spread in v_{r+m}, although v_{mt} would be comparable with or even dominant over $v_e \sin i$ at small values of v_{r+m} (say, 2–3 km s^{-1}).

Consequently, we may state that the stellar rotation (or the angular momentum) is closely/directly involved in the surface lithium abundance in the sense that higher A_{Li} (i.e., less depletion) is realized in rapider rotating (larger v_e) stars. Though this scenario is just the opposite to what is believed for hot early-type stars (i.e., rotation enhances mixing; see, e.g., Meynet 2000) and intuitively not straightforward, it is interesting that such a tendency was actually predicted from the theoretical side by Martín & Claret (1996) in their Li abundance study of pre-main sequence stars; i.e., rapid rotation significantly inhibits the depletion of Li. Therefore, it may be worth applying similar theoretical investigations to our mature solar-type stars, in order to see whether any significant v_e-dependence of A_{Li} may be reproduced. Furthermore, according to this scenario, the low-Li nature of planet-host stars might suggest that such stars may have lost their angular momenta in a way related to planets (during the formation phase?). Again, contributions of theoreticians are needed to examine this hypothesis.

5.3. Future tasks

We have thus found observational evidence that v_{r+m} (the width of the macrobroadening function) is responsible for the large dispersion of A_{Li} in solar-analog stars, which may further suggest that the Li depletion critically depends on the stellar rotation (angular momentum), and the trend of apparently lower Li abundances in stars with planets (compared to normal stars) might be interpreted in this connection. Yet, while such a finding is a significant first step, the complex behavior of Li abundances in these early G-type stars is still far from being well understood and important tasks remain to be worked out.

More effort should be made to clarify the nature of stellar rotation, in order to check our postulation that the v_{r+m}-dependence is really attributed to the rotation effect. Although it is not necessarily easy to establish the projected rotational velocity ($v_e \sin i$) separated from the macroturbulence, because the former is generally slowed down to a few km s^{-1} and is often comparable to (or even dominated by) the latter in this T_{eff} region, it may be practicable if data of very high quality (ca. *S/N* $\gtrsim$ 1000 and R ~ 100 000) are available, as has been sometimes carried out for the Sun by using the solar flux spectrum (e.g., Takeda 1995b).

Also, we should not forget the importance of activity-monitoring observations (e.g., the strength of Ca II H+K core emission), because they can provide a way of directly evaluating the equatorial rotation velocity (v_e) from the rotational moduration period of such activity indicators. The significance of such observations is also emphasized by the fact that the rotation rate is closely related to the stellar activity.

[13] There was a naive consideration that Li depletion progressively goes on with age even around this solar T_{eff} region, mainly from studies of open clusters (see, e.g., Fig. 5 of Hobbs & Pilachowski 1988, which was also quoted by Ryan 2000). However, it has become clear that the situation is not so simple, at least for comparatively aged stars like our sample (although comparatively young clusters such as Pleades and Hyades show a reasonable age/T_{eff}-dependence of A_{Li} without any large dispersion). For example, Pasquini et al. (1997) found a considerable spread of A_{Li} in a solar-age cluster M 67.

[14] This v_{r+m}-sensitive trend of A_{Li} is confirmed for the 26 selected solar-twin candidates (cf. Fig. A.1b in Appendix A) having similar values of stellar fundamental parameters, which may be counted as further evidence that A_{Li} is essentially determined by v_{r+m} around the solar T_{eff} region.

[15] Of course, since the actual contribution is $v_e \sin i$, the (unknown) inclination angle (i) comes as an uncertain factor. Yet, we can still make a statistical argument.

[16] This is mainly attributed to convective granular motions and typically has a depth-dependent value of ζ_{RT} ~ 2–4 km s^{-1} for the Sun (Takeda 1995b), where ζ_{RT} is the radial-tangential macroturbulent velocity dispersion. This corresponds to v_{mt} ~ 1–2 km s^{-1} in terms of the Gaussian-type macroturbulent velocity relevant here ($f_{mt}(v) \propto \exp[-(v/v_{mt})^2]$), according to the relation of $v_{mt} \simeq 0.4\zeta_{RT}$ (i.e., nearly the same *FWHM*s of broadening functions are realized under this condition; see, e.g., Fig. 17.5 of Gray 2005). More detailed information about the macroturbulent velocity distribution functions (in comparison with that of rotation) is given in Gray (1988).

The data points in the $A_{\rm Li}$ vs. $\Delta T_{\rm eff}$ distribution reported in this study should be further enriched by increasing the size of the sample. Especially, we are interested in clarifying the structure of the lower boundary zone (running from $A_{\rm Li} \sim 3$ at $\Delta T_{\rm eff} \sim +200$ K to $A_{\rm Li} \sim 1$ at $\Delta T_{\rm eff} \sim 0$ K): Does the narrow gap along this boundary really exist? Is the region below this line really a forbidden zone? In addition, as already mentioned in Sect. 5.1, stars located on this boundary line may deserve particularly intensive examination (including radial-velocity monitoring) because the possibility of being planet-host stars might be higher.

We require theoretical investigations to clarify the physical mechanism underlying the characteristic distributions of $A_{\rm Li}$, since they still remain as a puzzle. For example, regarding the connection between the Li depletion and the stellar angular momentum (i.e., slower rotation tends to enhance depletion, especially in relation to planet-host stars showing a trend of Li-deficiency), which is suggested from the close correlation between $A_{\rm Li}$ and $v_{\rm r+m}$, we need a firm theoretical basis specifically directed to solar-type stars, such as was done by Martín & Claret (1996) for pre-main sequence stars. Another important task would be to theoretically explain the existence of the slant lower-boundary of the $A_{\rm Li}$ distribution at $\Delta T_{\rm eff} \sim +200$–0 K; i.e., the reason why no star is allowed to exist below it, why it is so sensitive to $T_{\rm eff}$, etc.

6. Summary and conclusions

In order to investigate the puzzling behavior of the surface Li abundances known for solar-analog G-type stars (such as the large dispersion amounting to $\gtrsim$2 dex and the trend of systematically low Li seen in planet-host stars), we carried out an extensive spectroscopic study on the Li abundances as well as stellar parameters for 118 solar analog stars (selected by the photometric criteria of $0.62 \lesssim B-V \lesssim 0.67$ and $4.5 \lesssim M_V \lesssim 5.1$) based on the high-dispersion spectra obtained at Okayama Astrophysical Observatory.

The atmospheric parameters ($T_{\rm eff}$, $\log g$, $v_{\rm t}$, and [Fe/H]) were spectroscopically determined by using the equivalent widths of Fe I and Fe II lines following Paper I (absolute parameters) and Paper III (differential parameters). The ages/masses were estimated by comparing the positions on the theoretical HR diagram with theoretical stellar evolutionary tracks. Then, the macrobroadening parameter ($v_{\rm r+m}$; rotation plus macroturbulence) and the Li abundance ($A_{\rm Li}$) were established by the automatic spectrum-fitting analysis applied to the 6080–6089 Å region and $\sim$ 6707–6708 Å region (around the Li I doublet at 6707.8 Å), respectively.

The resulting $A_{\rm Li}$ vs. $T_{\rm eff}$ relation turned out to show a characteristic distribution (inverse-triangle shape) enclosed by two clear-cut boundaries (the slanted one running from ~5900 K to ~5800 K and the vertical one at ~5700 K), where our Sun is located around its lowest apex. Havig examined the possible dependence of $A_{\rm Li}$ upon various stellar parameters, we found that $A_{\rm Li}$ is clearly correlated with $v_{\rm r+m}$, which must be the most important key parameter responsible for the large dispersion.

With the reasonable assumption that the difference in stellar rotational velocity is mainly responsible for the variety of $v_{\rm r+m}$, we conclude that the stellar angular momentum plays the decisive role in determining the surface Li abundances of solar-analog stars in the $T_{\rm eff}$ range of ~5900–5700 K in the sense that slow rotation enhances the depletion, and the low-Li tendency of planet-host stars might be interpreted in this connection (i.e., slowed rotation).

Acknowledgements. We thank the staff of the Okayama Astrophysical Observatory for their kind support in the observations.

Appendix A: Solar twin[17] candidates

This subject has long been a matter of interest for stellar spectropists and not a few investigations have been made since 1970s; see, e.g., Cayrel de Strobel (1996) for a comprehensive review concerning earlier studies. Thanks to intensive studies done by several groups in the past decade, a few specific candidates for the "closest ever solar twin" are now known, such as 18 Sco (=HD 146233 = HIP 79672; Porto de Mello & da Silva 1997), HIP 78399 (=HD 143436; King et al. 2005), and HD 98618 (=HIP 55459; Meléndez et al. 2006). Also, Soubiran & Triaud (2004) reported the top-ten solar analogs in the ELODIE library by using the χ^2 test (i.e., search for stars having spectra as similar to the solar spectrum as possible), in which 18 Sco was ranked as the best solar-twin target with its highest resemblance.

The complete differential technique (Paper III), which we adopted to establish $\Delta T_{\rm eff}$, $\Delta \log g$, $\Delta v_{\rm t}$, and Δ\{Fe/H\} (cf. Sect. 3.1.2), is suitable for application to such a solar-twin survey, since such stars should have all these four Δ values as close as zero[18]. Therefore, from our 118 solar-analog targets, we selected 26 stars of particularly high resemblance to the Sun by the criterion that all four conditions of $|\Delta T_{\rm eff}| < 60$ K, $|\Delta \log g| < 0.15$, $|\Delta v_{\rm t}| < 0.1$ km s^{-1}, and $|\Delta\{{\rm Fe/H}\}| < 0.1$ are simultaneously satified (we chose these ranges rather arbitrarily by consulting the extents of their dispersions in Figs. 4a–c). The properties of these 26 stars are summarized in Table A.1, where the values of the similarity indicator (σ) defined as $\sigma^2 \equiv (\Delta T_{\rm eff}/60)^2 + (\Delta \log g/0.15)^2 + (\Delta v_{\rm t}/0.1)^2 + (\Delta\{{\rm Fe/H}\})^2$ are also given. In analogy with Fig. 13, the $A_{\rm Li}$ vs. $\Delta T_{\rm eff}$ and $A_{\rm Li}$ vs. $v_{\rm r+m}$ correlations are depicted in Fig. A.1. While these selected targets are considered to be similar to each other in terms of the four atmospheric parameters, we recognize from Fig. A.1 that their $A_{\rm Li}$ exhibit some trends with respect to $T_{\rm eff}$ and $v_{\rm r+m}$ even within such narrow parameter ranges (as already remarked at the footnotes in Sects. 5.2.1 and 5.2.2), which may imply a close connection between $T_{\rm eff}$ and $v_{\rm r+m}$. Such a $v_{\rm r+m}$-dependence of $A_{\rm Li}$ substatiates our argument presented in Sect. 5.2.2.

What is the most similar star to the Sun in our selected sub-sample? Regarding the three objects (HIP 79672, HIP 78399, and HIP 55459) reported as "very close solar-twins" by the above-mentioned studies, two of them (HIP 79672 and HIP 55459) are included in our selection with σ values of 0.309 and 0.591 (while we can not say anything about HIP 78399,

[17] We use the term "solar twin" for those special objects which have particularly high similarity to the Sun (even among the solar-analog group)with respect to spectra as well as stellar parameters.

[18] One might consider that the similarity of $T_{\rm eff}$, $\log g$, $v_{\rm t}$, and $A_{\rm Fe}$ cannot be a sufficient condition (though it is a necessary condition) for two stars being identical. Namely, even if the equalities of $T_{\rm eff,1} \simeq T_{\rm eff,2}$ and $g_1 \simeq g_2$ were observationally confirmed, the inequalities of $L_1 \neq L_2$ and $M_1 \neq M_2$ might in principle be possible in the coincidental case where $\log(L_1/L_2) \simeq \log(M_1/M_2)$ is satisfied (recall the relation of $\log(L_1/L_2) - \log(M_1/M_2) = 4\log(T_{\rm eff,1}/T_{\rm eff,2}) - \log(g_1/g_2)$). However, we confirmed by theoretical stellar evolutionary tracks that such equality and inequality relations in terms of L and M are never realized simultaneously (i.e., the $\log L$-difference is actually much larger than the $\log M$-difference) at the same $T_{\rm eff}$ and metallicity and thus this possibility can be excluded. In other words, two stars having the same values of these four atmospheric parameters may safely be considered to occupy the same position on the HR diagram; i.e., with the same age.

Table A.1. Selected stars with particularly high resemblance to the Sun.

Star	$\Delta T_{\rm eff}$	$\Delta \log g$	$\Delta v_{\rm t}$	Δ\{Fe/H\}	M	log *age*	Q_{age}	$v_{\rm r+m}$	$A_{\rm Li}$	$q_{\rm Li}$	σ
HIP 7585	+0.2	−0.009	+0.04	+0.067	1.02	9.68	A	2.66	1.84	a	0.391
HIP 8486	+30.2	−0.002	+0.09	−0.055	0.97	9.69	C	2.72	2.55	a	0.608
HIP 9349	+19.7	−0.064	+0.03	+0.012	1.00	9.73	A	2.60	2.06	a	0.332
HIP 11728	−50.7	−0.055	+0.01	+0.033	1.01	9.48	B	2.49	(<1.03)	x	0.492
HIP 19925	−19.5	+0.041	−0.01	+0.064	0.99	9.47	C	2.70	1.61	a	0.402
HIP 25002	−54.6	−0.029	+0.09	−0.096	0.99	9.56	C	3.53	2.38	a	0.806
HIP 31965	+10.2	−0.111	+0.01	+0.051	1.01	9.87	A	2.49	1.00	b	0.464
HIP 32673	−30.9	+0.138	−0.07	+0.075	1.02	9.50	B	2.28	(<1.04)	x	0.755
HIP 35265	+51.8	−0.055	+0.06	−0.009	1.00	9.79	A	2.24	2.01	a	0.559
HIP 38647	−48.3	−0.028	−0.03	+0.012	1.00	9.43	A	2.83	2.13	a	0.518
HIP 43557	+41.2	−0.030	+0.05	−0.061	1.00	9.80	A	3.43	1.50	a	0.579
HIP 49728	−21.1	−0.044	−0.02	−0.064	1.00	9.60	C	2.41	(<1.05)	x	0.422
HIP 49756	−35.1	−0.145	+0.01	+0.027	1.02	9.58	C	2.51	1.34	a	0.614
HIP 55459	+51.1	−0.037	+0.03	+0.072	1.03	9.58	A	2.70	1.58	a	0.591
HIP 59610	+59.1	−0.129	+0.07	−0.066	1.02	9.63	B	2.57	1.62	a	0.812
HIP 62816	+31.8	−0.028	−0.08	+0.069	1.02	9.49	B	3.68	2.16	a	0.624
HIP 64150	−14.4	+0.014	+0.03	+0.067	1.04	9.63	B	2.56	(<1.04)	x	0.397
HIP 75676	−6.0	−0.031	−0.08	−0.090	0.98	9.62	A	2.54	(<1.07)	x	0.614
HIP 76114	−34.0	+0.056	+0.00	−0.003	1.01	9.59	C	2.23	0.91	b	0.388
HIP 79672	+1.7	−0.056	−0.03	+0.039	1.02	9.66	A	2.66	1.63	a	0.309
HIP 88194	−49.2	−0.043	+0.01	−0.071	0.97	9.67	C	2.25	(<0.83)	x	0.625
HIP 96901	−24.2	−0.121	+0.00	+0.086	1.01	9.77	B	2.38	(<1.06)	x	0.637
HIP 96948	−8.8	−0.003	+0.06	+0.097	1.04	9.62	C	2.30	1.52	a	0.577
HIP 97420	+32.3	+0.002	+0.04	+0.064	1.01	9.65	B	2.84	2.22	a	0.497
HIP 100963	−1.6	−0.026	−0.02	−0.012	1.00	9.71	A	2.70	1.72	a	0.146
HIP 112504	−16.0	−0.064	−0.01	+0.020	1.02	9.63	C	2.40	2.01	a	0.289

Note. The Δ values are the parameter differences (relative to the Sun) for $T_{\rm eff}$ (K), $\log g$ (dex), $v_{\rm t}$ (km s^{-1}), and {Fe/H} (dex), which were derived as results from the complete differential analysis (Sect. 3.1.2). The units of the other quantities are as follows: M (in $M_\odot$), *age* (in yr), $v_{\rm r+m}$ (in km s^{-1}), $A_{\rm Li}$ (with the normalization of $A_{\rm H} = 12.00$). See the text for more details regarding the age-reliability class (Q_{age}; Sect. 3.3), the grade of $A_{\rm Li}$-determination ($q_{\rm Li}$; Sect. 4.3), and the relative-to-Sun similarity index (σ; Appendix A).

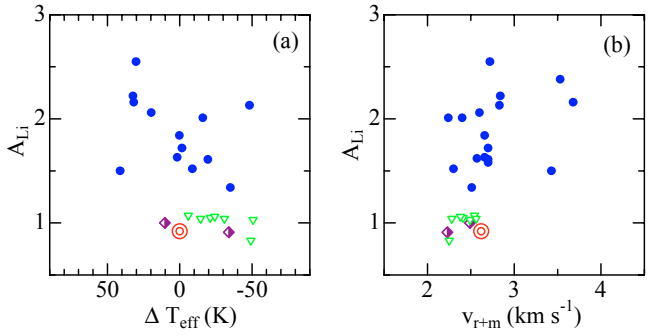

Fig. A.1. Plots of $A_{\rm Li}$ vs. $\Delta T_{\rm eff}$ (*left panel* **a**)) and $A_{\rm Li}$ vs. $v_{\rm r+m}$ (*right panel* **b**)) correlations for the 26 stars showing particularly high similarities to the Sun (with respect to the stellar parameters) among our sample stars (cf. Table A.1). See the caption of Fig. 9a for the meanings of the symbols.

since it was not observed). However, among the 28 objects in Table A.1, the closest Sun-like star is HIP 110963 with the smallest σ of 0.146. Since its similarity to the Sun has never been reported so far (at least to our knowledge), we propose this star as another very good solar-twin candidate. The remarkable resemblance of the spectra between HIP 110963 and the Sun is demonstrated in Fig. A.2, where the spectrum of HIP 79672 (=18 Sco; the top-ranked solar twin in the top-ten list of Soubiran & Triaud 2004) is also shown for comparison. Thus, HIP 110963 equally deserves the name of "closest-ever solar twin".

However, all these good solar-twin candidates (HIP 110963, HIP 79672, HIP 78399, and HIP 55459) are markedly different from the Sun in terms of the Li I 6708 line strength (or the surface Li abundance) in spite of the striking similarity of fundamental stellar parameters; that is, their $A_{\rm Li}$ values of 1.5–1.8 (cf. Table A.1; King et al. 2005 for HIP 78399) are significantly larger than $A_{\rm Li,\odot}$ of 0.92 (Paper II), which is clearly recognized also by visual inspection of the spectra (e.g., Fig. A.2). According to the tentative conclusion in Sect. 5.2.2 that stellar rotation may be the key parameter[19] responsible for producing a variety of $A_{\rm Li}$, we speculate that the rotational velocities of these stars may be larger than the solar $v_{\rm e}$ of 2.0 km s^{-1} (siderial value; or 1.86 km s^{-1} in the synodic case). It would be worth trying to check this hypothesis observationally as proposed in Sect. 5.3.

Somewhat ironically, stars with very high relative-to-Sun similarities of stellar parameters show considerably different/stronger Li line strengths, while the coincidence of stellar parameters is not satisfactory for those showing very weak Li feature like the Sun. This fact makes us wonder whether such

[19] This argument may be supported by a consideration from a more fundamental point of view. That is, recent stellar evolution theory tells us that any two stars should be identical if the (1) initial angular momentum, (2) initial mass, (3) initial chemical composition, and (4) age, are the same for both. Then, if the atmospheric parameters ($T_{\rm eff}$, $\log g$, $v_{\rm t}$, and $A_{\rm Fe}$) are equal, the similarity of (2)–(4) is automatically guaranteed (because the same position on the theoretical HR diagram is occupied with the same metallicity). In such a case, the only possible reason that can produce different characteristics between two stars would be the difference in (1); i.e., stellar rotation.

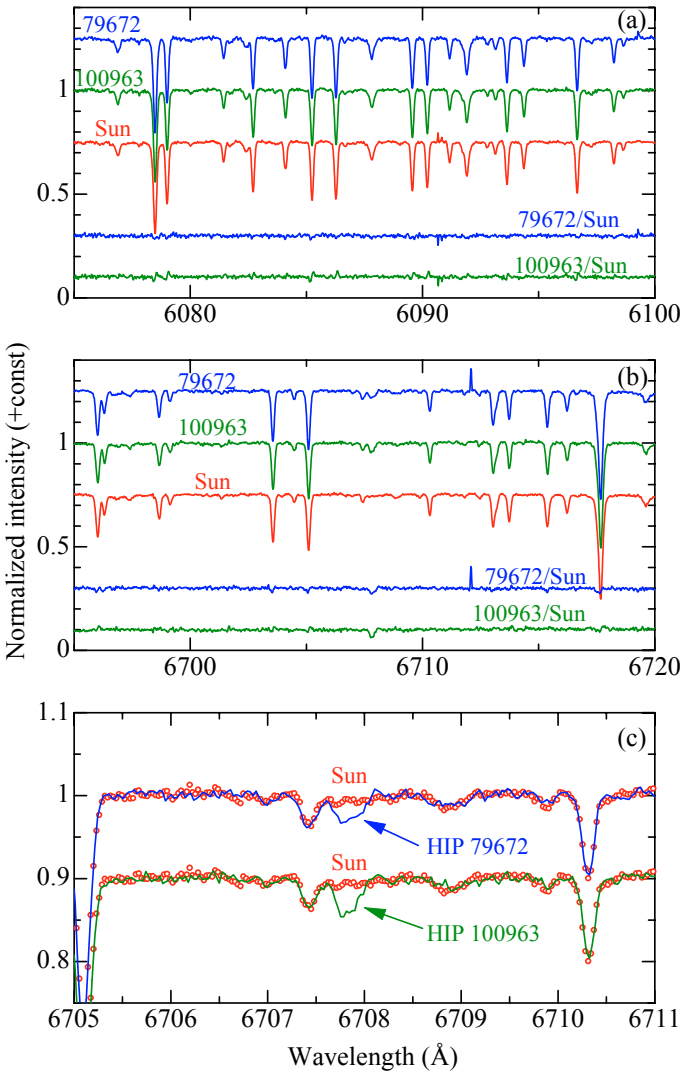

Fig. A.2. Comparison of the spectrum portions of HIP 79672 (=18 Sco; one of the closest-ever solar twins; cf. Porto de Mello & da Silva 1997; and Soubiran & Triaud 2004), HIP 100963 (another closet-class candidate newly nominated in this study), and the Sun: **a)** 6075–6100 Å region, **b)** 6695–6720 Å region, and **c)** 6705–6711 Å region. An appropriate vertical offset is applied to each spectrum (0.25 in **a)** and **b)**, and 0.1 in **c)**). In the lower parts of panels **a)** and **b)**, the star/Sun residuals are also displayed to demonstrate their remarkable similarity to the solar spectrum.

an ideal solar twin ever exists that satisfying both requirements, which is related to the question "Is our Sun normal or peculiar when it is seen as a star and compared to other solar analogs?" (see also Gustafsson 1998 or Giampapa 2005).

References

Alonso, A., Arribas, S., & Martínes-Roger, C. 1996, A&A, 313, 873
Arenou, F., Grenon, M., & Gómez, A. 1992, A&A, 258, 104
Cayrel, R. 1988, in The Impact of Very High *S/N* Spectroscopy on Stellar Physics, ed. G. Cayrel de Strobel, & M. Spite (Dordrecht: Kluwer), Proc. IAU Symp, 132, 345
Cayrel de Strobel, G. 1996, A&ARv, 7, 243
Chen, Y. Q., Nissen, P. E., Benoni, T., & Zhao, G. 2001, A&A, 371, 943
Chen, Y. Q., & Zhao, G. 2006, AJ, 131, 1816
Cox, A. N. 1999, Allen's Astrophysical Quantities, 4th edn. (Springer)
Dias, W. S., Alessi, B. S., Moitinho, A., & Lépine, J. R. D. 2002, A&A, 389, 871
Domínguez Cerdeña, C., Rebolo, R., Israelian, G., Ecuvillon, A., & Santos, N. 2006, Poster presented in the conference, The Metal-Rich Universe, La Palma, Spain
ESA 1997, The Hipparcos and Tycho Catalogues, ESA SP-1200, available from NASA-ADC or CDS in a machine-readable form (file name: `hip_main.dat`)
Favata, F., Micela, G., & Sciortino, S. 1996, A&A, 311, 951
Galeev, A. I., Bikmaev, I. F., Mashonkina, L. I., Musaev, F. A., & Galazutdinov, G. A. 2004, Astron. Rep., 48, 511
Giampapa, M. 2005, in The Sun, Solar Analogs, and the Climate, Saas-Fee Advances Course 34/2004 (Berlin: Springer), 307
Girardi, L., Bressan, A., Bertelli, G., & Chiosi, C. 2000, A&AS, 141, 371, `http://pleiadi.pd.astro.it/`
Gonzalez, G., & Laws, C. 2000, AJ, 119, 390
Gray, D. F. 1988, Lectures on Spectral-Line Analysis: F, G, and K Stars (Arva, Ontario: The Publisher)
Gray, D. F. 2005, The Observation and Analysis of Stellar Photospheres, 3rd edn. (Cambridge: Cambridge University Press)
Gustafsson, B. 1998, Sp. Sci. Rev., 85, 419
Hobbs, L. M., & Pilachowski, C. 1988, ApJ, 334, 734
Ibukiyama, A., & Arimoto, N. 2002, A&A, 394, 927
Israelian, G., Santos, N. C., Mayor, M., & Rebolo, R. 2004, A&A, 414, 601
Izumiura, H. 1999, in Proc. 4th East Asian Meeting on Astronomy, Observational Astrophysics in Asia and its Future ed. P. S. Chen (Kunming: Yunnan Observatory), 77
King, J. R., Deliyannis, C. P., Hiltgen, D. D., et al. 1997, AJ, 113, 1871
King, J. R., Boesgaard, A. M., & Schuler, S. C. 2005, AJ, 130, 2318
Kurucz, R. L. 1993, Kurucz CD-ROM, No. 13, Harvard-Smithsonian Center for Astrophysics, `http://kurucz.harvard.edu/grids.html`
Lambert, D. L., & Reddy, B. E. 2004, MNRAS, 349, 757
Luck, R. E., & Heiter, U. 2006, AJ, 131, 3069
Mallik, S. V., Parthasarathy, M., & Pati, A. K. 2003, A&A, 409, 251
Martín, E. L., & Claret, A. 1996, A&A, 306, 408
Meléndez, J., Dodds-Eden, K., & Robles, J. A. 2006, ApJ, 641, L133
Meynet, G. 2000, in Stellar Clusters and Associations: Convection, Rotation, and Dynamos, ed. R. Pallavicini, G. Micela, & S. Sciortino (San Francisco: ASP), ASP Conf. Ser., 198, 3
Pasquini, L., Liu, Q., & Pallavicini, R. 1994, A&A, 287, 191
Pasquini, L., Randich, S., & Pallavicini, R. 1997, A&A, 325, 535
Porto de Mello, G. F., & da Silva, L. 1997, ApJ, 482, L89
Qiu, H. M., Zhao, G., & Li, Z. W. 2001, Ap&SS, 277, 565
Ryan, S. G. 2000, MNRAS, 316, L35
Soubiran, C., & Triaud, A. 2004, A&A, 418, 1089
Takeda, Y. 1995a, PASJ, 47, 287
Takeda, Y. 1995b, PASJ, 47, 337
Takeda, Y. 2005, PASJ, 57, 83 (Paper III)
Takeda, Y. 2007, PASJ, 59, 335 (Paper IV)
Takeda, Y., & Kawanomoto, S. 2005, PASJ, 57, 45 (Paper II)
Takeda, Y., Sato, B., Kambe, E., et al. 2001, PASJ, 53, 1211
Takeda, Y., Ohkubo, M., & Sadakane, K. 2002, PASJ, 54, 451
Takeda, Y., Sato, B., Kambe, E., et al. 2005a, PASJ, 57, 13
Takeda, Y., Ohkubo, M., Sato, B., Kambe, E., & Sadakane, K. 2005b, PASJ, 57, 27 (Paper I) [Erratum: PASJ, 57, 415]